Theoretical and Experimental Studies of Anisotropic Shrinkage in Injection Moldings of Various Polyesters

Keehae Kwon, A. I. Isayev, K. H. Kim

Institute of Polymer Engineering, The University of Akron, Akron, Ohio 44325 0301

Received 16 March 2006; accepted 17 May 2006
DOI 10.1002/app.24807
Published online in Wiley InterScience (www.interscience.wiley.com).

ABSTRACT: A novel approach to predict anisotropic shrinkage of slow crystallizing polymers in injection moldings was proposed, using the flow-induced crystallization, frozen-in molecular orientation, elastic recovery, and PVT equation of state. In the present study, three different polyesters, polyethylene terephthalate, polybutylene terephthalate, and polyethylene-2,6-naphthalate (PEN), are used. The anisotropic thermal expansion and compressibility affected by the frozen-in orientation function and the elastic recovery that was not frozen during moldings were introduced to obtain the in-plane anisotropic shrinkages. The frozen-in orientation function was calculated from the amorphous contribution based on the frozen-in and intrinsic amorphous birefringence and crystalline contribution based on the crystalline orientation function determined from the elastic recovery and intrinsic crystalline birefringence. To model the elastic recovery and frozen-in stresses related to birefringence during molding process, a nonlinear viscoelastic constitutive equation was used with the temperature-dependent viscosity and relaxation time. Occurrence of the flow-induced crystallization was introduced through the elevation of melting temperature affected by entropy production during flow of the viscoelastic melt. Kinetics of the crystallization was modeled using Nakamura and Hoffman-Lauritzen equations with the rate constant affected by the elevated melting temperature. Numerous injection molding runs were carried out by varying the packing time, packing pressure, flow rate, melt and mold temperature, and anisotropic shrinkage of moldings were measured. The experimental results were compared with the simulated data and found in a fair agreement. © 2006 Wiley Periodicals, Inc. J Appl Polym Sci 102: 3526–3544, 2006

Key words: crystallization; injection molding; polyester; shrinkage; simulation

INTRODUCTION

Shrinkage of injection molded parts of semicrystalline thermoplastics is affected by the volumetric shrinkage, flow-induced residual stresses and orientation, flow-induced crystallization, and heat transfer. Since all these factors are influenced by the processing conditions such as packing pressure, packing time, melt temperature, mold temperature, injection speed, and material properties as well as geometric constraints, the prediction of shrinkage, especially of anisotropic linear shrinkage, is quite complex issue. Clearly the shrinkage anisotropy in moldings cannot be predicted based on volume shrinkage alone. Therefore, novel methodology for accurate prediction of anisotropic shrinkage in moldings is required.

For slow-crystallizing polymers such as polyesters, the developed crystallinity during molding is very low because of the slow crystallization rate and therefore, under typical molding conditions, the ultimate crystallinity cannot be achieved. Also, the shrinkage of each layer would vary in accordance with the developed crystallinity. Since the developed crystallinity remains low during molding, the contribution of amorphous region plays a dominant rule in the shrinkage of slow crystallizing polymers. This is in contrast to the fast crystallizing polymers where the ultimate crystallinity can be achieved during typical molding conditions.

A number of mathematical models have been proposed for the simulation of quiescent crystallization.[1–6] Most of the nonisothermal crystallization theories[1–4] have been developed based upon Avrami-Kolmogoroff theory for the isothermal crystallization.[5,6] Nakamura et al.[2,3] extended the theories of isothermal crystallization to nonisothermal quiescent crystallization, which is customarily cited in literature as ''Nakamura model.'' Quiescent crystallization kinetics for polyethylene terephthalate (PET) samples by the isothermal[7] and the nonisothermal[8] DSC analysis were extensively studied. The measured DSC data was fitted with Nakamura[2] and Hoffman-Lauritzen[1] equation to obtain the model parameters of quiescent crystallization kinetics. However, in polymer processing, because of the flow-induced crystallization, the morphology developed in the final product is typically very different from that observed as a result of quiescent crystallization.

Correspondence to: A. I. Isayev (aisayev@uakron.edu).
Contract grant sponsor: National Science Foundation, Division of Engineering; contract grant number: DMI-0322920.

The statistical mechanical model expressing the melting point elevation was first quantified by Flory[9] in his classic derivation of the equilibrium transition temperature for a stretched, crosslinked system. Similar concepts of melting temperature elevation of flow-induced crystallization were developed by other researchers.[10–13] Dunning[10] was the first one who introduced the concept of melting temperature elevation, due to crystallization, into the rate of crystal growth and nucleation. Flory's Gaussian expression was later modified by Gaylord[13] who applied the concepts of irreversible thermodynamics to determine the crystallization rates using non-Gaussian concepts.

Much research for flow-induced and quiescent crystallization has been done.[14–21] In particular, a method to predict the skin layer thickenss in the injection moldings of isotactic polypropylene was proposed using the modification of Janeschitz-Kriegl model of flow-induced crystallization.[14,15] In addition, a unified crystallization model was proposed to describe the phenomena under nonisothermal flow conditions.[16,17] An attempt was also made to incorporate influences of the viscoelastic behavior of semicrystalline polymers on flow-induced crystallization.[18–21] The approach to the flow-induced crystallization was based on the thermodynamical consideration. The elevated melting temperature was determined by calculating the reduction of entropy between the oriented and unoriented melts using the nonlinear viscoelastic constitutive equation. This temperature was incorporated into the Nakamura nonisothermal crystallization equation.

A rapid nonhomogeneous cooling of a crystalline polymer melt through the melting temperature introduces volumetric shrinkage. By following the PVT diagram from the melt temperature to ambient conditions, one can obtain the average value of the final product volume.[22–24] However, this approach to calculate shrinkage is limited because the PVT diagram is suitable to describe isotropic shrinkage only.

Recently, several new approaches were proposed to predict anisotropic shrinkage for amorphous and fast crystallizing polymers.[25–32] Thermoviscoelastic material model to predict the part shrinkage, warpage, and the build-up of residual stresses in the injection molding process was used.[25,26] However, flow effect was neglected and in-plane shrinkages were assumed to be equal. A simple thermoelastic model taking into account thermal and pressure effect on in-plane shrinkage and Poisson's ratio on thickness shrinkage was also proposed.[27–30] The PVT behavior affected by crystallinity, dependent upon the thermal, pressure and shear stress history was used.[31] On the basis of the modified material constants, the time-dependent gapwise shrinkage of molded specimen prior to ejection from the cavity was calculated and compared with measured data. Recently, residual strain and thermoviscoelastic stress model was used to calculate the shrinkage coefficient and to predict the in-plane shrinkage in the parallel and transverse to the flow direction.[32] However, to improve the prediction of shrinkage and warpage, a hybrid model was used.

For slow crystallizing polymers, only a few studies were done to predict shrinkage. Volumetric shrinkage was predicted based on PVT equation of state and the results were compared with the experimental data for PET moldings at different packing pressure, melt temperature and mold temperature. However, the flow-induced crystallization and viscoelastic effects were neglected.

In the present study, an approach developed earlier to predict the anisotropic shrinkage of injection molded products of amorphous[33] and fast crystallizing[34] polymers was expended to describe anisotropic shrinkage of slow crystallizing polymers. This description is based on the frozen-in orientation function and elastic recovery determined from a nonlinear constitutive equation. Numerical simulation of viscoelastic injection molding process including filling, packing and cooling stages was developed. The crystallization rate enhanced by flow effect was included by the incorporation of elevated equilibrium melting temperature into the Nakamura and Hoffman-Lauritzen equation. The amorphous and crystalline contribution to the total thermal contraction was independently considered, since the amorphous and crystalline regions were frozen at different temperature. To calculate frozen-in orientation, elastic recovery and elevated melting temperature, a nonlinear viscoelastic constitutive equation was used. Various polyesters were used as representatives of slow [PET, polyethylene-2,6-naphthalate (PEN)] and intermediate (polybutylene terephthalate, PBT) crystallizing polymers. The predicted anisotropic shrinkages were compared with the experimental results measured at various processing conditions and found to be in a good agreement.

THEORETICAL

Governing equations

The general behavior for a compressible, nonisothermal flow is described by transport equations: mass, momentum and energy equation. The continuity and momentum equation are given by

$$\frac{\partial \rho}{\partial t} + \nabla \rho \boldsymbol{v} = 0 \tag{1}$$

$$\frac{\partial \rho v}{\partial t} + \boldsymbol{v} \cdot \nabla \rho \boldsymbol{v} = -\nabla P - \nabla \cdot \tau \tag{2}$$

where ρ is density, $\boldsymbol{v}$ is the velocity vector, P is the pressure, and $\boldsymbol{\tau}$ is the stress tensor.

A multimode viscoelastic constitutive equation[35,36] is used to describe the rheological behavior of polymer melts as

$$\overset{\nabla}{\boldsymbol{C}}_k + \frac{1}{2\theta_k}\left[\boldsymbol{C}_k^2 + \frac{1}{3}(II_C^k - I_C^k)\boldsymbol{C}_k - \boldsymbol{I}\right] = 0 \tag{3}$$

where $\boldsymbol{C}_k$ is the elastic strain tensor in the kth mode, $\overset{\nabla}{\boldsymbol{C}}_k$ is the Jaumann derivative of the elastic strain tensor, $\boldsymbol{I}$ is the identity tensor and I_C^k and II_C^k are the first and the second invariant of the elastic strain tensor, $\boldsymbol{C}_k$.

In a nonisothermal flow under consideration, the energy equation is

$$\rho C_p\left(\frac{\partial T}{\partial t} + \boldsymbol{v}\cdot\nabla T\right) = k\nabla^2 T + \Phi + \dot{Q} \tag{4}$$

where C_p is the specific heat, k is the thermal conductivity and $\dot{Q}$ is the rate of heat generated by crystallization as

$$\dot{Q} = \rho X_\infty \Delta H_c \frac{d\theta}{dt} \tag{5}$$

where X_∞ is the ultimate degree of crystallinity, ΔH_c is the heat of fusion per unit mass for the ideal 100% crystalline state and θ is the relative crystallinity.

The energy dissipation function for viscoelastic flow[37] is calculated as

$$\Phi = 2s\eta_0\,\mathrm{tr}(\boldsymbol{e}^2) + \sum_{k=1}^{N}\frac{\eta_k}{4\theta_k^2}\left[\frac{1}{3}\mathrm{tr}\boldsymbol{C}_k\cdot\{\mathrm{tr}(\boldsymbol{C}_k^{-1}) - \mathrm{tr}\boldsymbol{C}_k\} + \mathrm{tr}(\boldsymbol{C}_k^2) - 3\right] \tag{6}$$

where s is the nondimensional rheological parameter between 0 and 1, $\boldsymbol{e}$ is the deformation-rate tensor, η_k and θ_k are the viscosity and relaxation time in the kth mode and η_0 is the zero-shear viscosity such as

$$\eta_0(T) = \frac{\sum_{k=1}^{N}\eta_k(T)}{1-s} \tag{7}$$

The temperature-dependence of viscosity and relaxation time in the kth mode is expressed by the Arrhenius-type equation:

$$\eta_k(T) = A_k\,\exp\left(\frac{T_b}{T}\right), \quad \theta_k(T) = B_k\exp\left(\frac{T_b}{T}\right) \tag{8}$$

where T_b is the temperature sensitivity related to the activation energy and A_k, B_k are constants.

In this research, following assumptions are made for the simulation of injection molding process:

a. The thin film approximation.
b. No slip condition at the wall.
c. No the inertial and body force in the momentum equation.
d. Thermal conduction in the flow direction is negligible with respect to conduction in the thickness direction.
e. No fountain flow effect at the melt front.

For one-dimensional incompressible flow in the filling stage, eqs. (1) and (2) are expressed as:[38]

$$\frac{\partial}{\partial x}\left(S\frac{\partial P}{\partial x}\right) = 0 \tag{9}$$

where x is the flow direction and S is the fluidity expressed as

$$S = \int_0^b \frac{z^2}{\eta}dz \qquad \text{in Cartesian coordinates} \tag{10}$$

$$S = \frac{1}{2}\int_0^R \frac{r^3}{\eta}dr \qquad \text{in cylindrical coordinates} \tag{11}$$

where z and r are the thickness and radial directions, b is the half thickness of the cavity, R is the radius of the tube.

In case of simple shear flow, the elastic strain tensor has the following form:

$$\boldsymbol{C}_k = \begin{bmatrix} C_{11,k} & C_{12,k} & 0 \\ C_{12,k} & C_{22,k} & 0 \\ 0 & 0 & 1 \end{bmatrix} \tag{12}$$

Therefore, the stress tensor, τ, is expressed as

$$\boldsymbol{\tau}(x,z,t) = 2\mu\theta_1(T)s\dot{\gamma}\begin{bmatrix} 0 & 1 & 0 \\ 1 & 0 & 0 \\ 0 & 0 & 0 \end{bmatrix} + 2\sum_{k=1}^{N}\mu_k(T)\begin{bmatrix} C_{11,k} & C_{12,k} & 0 \\ C_{12,k} & C_{22,k} & 0 \\ 0 & 0 & 1 \end{bmatrix} \tag{13}$$

where $\dot{\gamma} = \partial v_x/\partial z$ is the shear rate with v_x being the velocity in the flow direction, $\mu_k = \eta_k/2\theta_k$ is the modulus of kth mode and $\mu = \eta_0/2\theta_1$.

The gapwise average velocity, $\overline{v}_x$, is expressed as

$$\overline{v}_x = \frac{1}{b}\int_0^b v_x\,dz \tag{14}$$

The governing equation for $\boldsymbol{C}_k$ in eq. (3) is expressed as follows:

$$\frac{DC_{11,k}}{Dt} - 2C_{12,k}\frac{\partial v_x}{\partial z} + \frac{1}{2\theta_k}(C_{11,k}^2 + C_{12,k}^2 - 1) = 0 \tag{15}$$

$$\frac{DC_{12,k}}{Dt} - C_{22,k}\frac{\partial v_x}{\partial z} + \frac{1}{2\theta_k}(C_{11,k} + C_{22,k})C_{12,k} = 0 \quad (16)$$

$$C_{11,k}C_{22,k} - C_{12,k}^2 = 1 \quad (17)$$

where D/Dt is the material derivative operator.

The shear stress, τ_{12}, is expressed as

$$\tau_{12} = \Lambda_x z = \eta\dot{\gamma}, \quad \Lambda_x = -\frac{\partial P}{\partial x} \quad (18)$$

By intergrating eq. (14) by part and eliminating $\dot{\gamma}$ with aid of eq. (18), the average velocity, $\overline{v}_x$, is expressed as

$$\overline{v}_x = \frac{\Lambda_x}{b}\int_0^b \frac{z^2}{\eta}dz = \frac{\Lambda_x}{b}S \quad (19)$$

From eqs. (13), (14), and (19) Λ_x is given as

$$\Lambda_x = \frac{\left(2\mu s\overline{v}_x - 2\sum_{k=1}^{N}\mu_k\int_0^b \frac{zC_{12,k}}{\theta_1}dz\right)}{\int_0^b \frac{z^2}{\theta_1}dz} \quad (20)$$

The elastic strain tensor components at a steady state flow, $\boldsymbol{C}_k^{\mathrm{st}}$, are given by:[35]

$$C_{11,k}^{\mathrm{st}} = \frac{\sqrt{2}X_k}{\sqrt{1+X_k}} \quad (21)$$

$$C_{12,k}^{\mathrm{st}} = \frac{2\dot{\gamma}X_k}{1+X_k} \quad (22)$$

$$C_{22,k}^{\mathrm{st}} = \frac{\sqrt{2}}{\sqrt{1+X_k}} \quad (23)$$

where $X_k = 1 + \sqrt{1+4(\dot{\gamma}\theta_k)^2}$.

The shear viscosity is expressed as

$$\eta = \eta_0 s + \sum_{k=1}^{N}\frac{2\eta_k}{1+\sqrt{1+4(\dot{\gamma}\theta_k)^2}} \quad (24)$$

During the packing stage, an extra material is forced into the cavity to compensate for volume shrinkage due to solidification. The packing pressure is built up and the corresponding density is increased. To calculate pressure build up during the packing stage and pressure decay during the cooling stage, the following equation[38] is used:

$$G(x,t)\frac{\partial P}{\partial t} + \frac{1}{b}\frac{\partial(S\Lambda_x)}{\partial x} = -F(x,t) \quad (25)$$

where

$$G(x,t) = \frac{1}{b}\left(\frac{1}{P+\overline{P}}\right)\int_0^b\left(1-\frac{\rho}{\overline{\rho}}\right)dz \quad (26)$$

$$F(x,t) = -\frac{1}{b}\int_0^b\left(1-\frac{\rho}{\overline{\rho}}\right)\frac{\partial \ln T}{\partial t}dz \quad (27)$$

Equations (25)–(27) are the unified formulation for filling, packing and cooling stages. During the filling stage, $F(x,t)$ and $G(x,t)$ are negligible. Therefore, eq. (25) is reduced to eq. (9). During the packing stage, $G(x,t)$ is important while $F(x,t)$ is negligible. During the cooling stage, both $F(x,t)$ and $G(x,t)$ become important.

Flow-induced crystallization

For an oriented polymer melt, the reduction in entropy, due to the orientation of polymer molecules under flow, causes the elevation of equilibrium melting point, T_m^0. According to Flory,[9] the elevated melting temperature, T_m, is calculated as

$$\frac{1}{T_m} = \frac{1}{T_m^0} - \frac{\Delta S}{\Delta H_f} \quad (28)$$

where ΔS is the change of entropy and ΔH_f is the change of enthalpy of crystallization which is defined as the difference between the heat released by crystallization, ΔH_f^m, and the created interfacial energy, ΔH_f^A as

$$\Delta H_f = \Delta H_f^m - \Delta H_f^A = f_{\mathrm{cr}}\,\Delta H_f^m \quad (29)$$

The crystallization factor, f_{cr}, is introduced as the crystallization enthalpy change divided by the heat of crystallization. Evidently, since the crystallization factor is affected by the created interfacial energy, this value is very important in the flow-induced crystallization. Accordingly, the temperature elevation by the oriented polymer melt is expressed as[18–21]

$$\frac{1}{T_m} = \frac{1}{T_m^0} - \frac{\Delta S}{f_{\mathrm{cr}}\,\Delta H_f^m} \quad (30)$$

The entropy reduction in eq. (30) is related to the first invariant of kth mode of the elastic strain tensor, I_C^k, as[18]

$$\Delta S = \sum_k \frac{\mu_k}{T\rho}(I_C^k - 3) \quad (31)$$

where $I_C^k = C_{11,k} + C_{22,k} + C_{33,k}$.

The flow-induced crystallization rates is introduced by replacing the equilibrium melting temperature, T_m^0,

in Nakamura equation[2] by means of the elevated melting temperature, T_m as[18–21]

$$\frac{d\theta}{dt} = nK_s(\dot{\gamma}, T)(1-\theta)[-\ln(1-\theta)]^{(n-1)/n} \quad (32)$$

where n is Avrami exponent, θ is the relative crystallinity, and $K_s(T, \dot{\gamma})$ is the modified crystallization rate constant affected by the shear rate as

$$K_s(\dot{\gamma}, T) = (\ln 2)^{1/n}\left(\frac{1}{t_{1/2}}\right)_0 \times \exp\left(\frac{-U^*/R}{T-T_\infty}\right)\exp\left(-\frac{K_k}{T(T_m(\dot{\gamma})-T)f}\right) \quad (33)$$

$$\text{with } f = \frac{2T}{T+T_m(\dot{\gamma})}, \quad T_\infty = T_g - 30$$

where f is the correction factor for the reduction in the latent heat of fusion as the temperature is decreased, R is the universal gas constant, U^* is the activation energy for segmental jump of polymer molecules assigned a universal value of 6284 J/mol, $(1/t_{1/2})_0$ is the pre-exponential factor that includes all terms influencing the crystallization process but independent of temperature and K_k is the nucleation exponent.

Orientation function, elastic recovery, and anisotropic properties

In case of slow crystallizing polymers, the amorphous and crystalline contribution to the total thermal contraction is independently considered since the amorphous and crystalline region are frozen at different temperatures. Therefore, the amorphous, f^a_{or}, and crystalline, f^c_{or}, orientation functions are calculated separately by using the following assumptions:

1. Uniaxial orientation

$$f^a_{or,1} = \frac{\Delta n_a}{\Delta n^0_a}, \quad f^c_{or,1} = f_c \quad (34)$$

2. Biaxial orientation

$$f^a_{or,1} = \frac{\Delta n_a}{\Delta n^0_a}, \quad f^a_{or,2} = \frac{(n_{22}-n_{33})_a}{\Delta n^0_a}$$
$$f^c_{or,1} = f^c_{or,2} = f_c \quad (35)$$

where Δn^0_a is the intrinsic amorphous birefringence and Δn_a and $(n_{22} - n_{33})_a$ are the birefringence in the amorphous region. The latter values are calculated from the following equations:

$$\Delta n_a \cong \Delta n^{fl}_a = C_\sigma\sqrt{N_1^2 + 4\tau_{12}^2} \quad (36)$$

$$(n_{22}-n_{33})_a \cong (n_{22}-n_{33})^{fl}_a = C_\sigma \cdot N_2 \quad (37)$$

where C_σ is the stress-optical coefficient. The value of frozen-in normal, N_1 and N_2, and shear, τ_{12}, stresses are calculated by eq. (13).

The crystalline orientation function is obtained through an elastic recovery. The magnitude of the elastic recovery is calculated as the total shear strain recovered after unloading the shear stress. The transient, γ_t, and the ultimate, γ_∞, elastic recovery are expressed as[39]

$$\gamma_t(t) = \int_0^t \dot{\gamma}_e(\xi)d\xi, \quad \gamma_\infty = \int_0^\infty \dot{\gamma}_e(\xi)d\xi \quad (38)$$

The shear rate during recovery is calculated from eq. (13) by letting shear stresses to zero as

$$\dot{\gamma}_e(t) = \frac{\sum_{k=1}^{N}\mu_k C_{xy,k}}{\mu s\theta_1} \quad (39)$$

Then the crystalline orientation function as a function of the principal extension ratio is calculated as suggested by Gaylord[13]

$$f_c = \frac{1}{2}\left(\frac{3\lambda^3}{2+\lambda^3} - 1\right) \quad (40)$$

where the principal extension ratio, λ, is expressed in terms of the ultimate elastic recovery in the simple shear flow as[40]

$$\lambda = \frac{\gamma_\infty + \sqrt{\gamma_\infty^2 + 4}}{2} \quad (41)$$

Then, the total orientation function is calculated:

$$f_{or,1} = (1-\chi)f^a_{or,1} + \chi f_c \quad (42)$$

$$f_{or,2} = (1-\chi)f^a_{or,2} + \chi f_c \quad (43)$$

where χ is the absolute crystallinity.

From the calculated orientation function, the anisotropic linear thermal expansion coefficient (LTEC) and compressibility are calculated based on the different orientation assumptions.[33,41,42] For slow crystallizing polymers, since the amorphous and crystalline regions are frozen at different temperatures and the developed crystallinity is low, the amorphous and crystalline contribution to the total thermal contraction is separately considered. From the calculated orientation functions, anisotropic LTEC and compressibility are calculated for amorphous and crystalline phases, respectively:

1. Uniaxial orientation

$$\alpha_x^a = \alpha_0(1 - f_{\mathrm{or},1}^a), \quad \alpha_y^a = \alpha_0\left(1 + \frac{f_{\mathrm{or},1}^a}{2}\right) \tag{44}$$

$$\alpha_x^c = \alpha_0(1 - f_c), \quad \alpha_y^c = \alpha_0\left(1 + \frac{f_c}{2}\right) \tag{45}$$

$$\beta_x = \beta_0(1 - f_{\mathrm{or},1}), \quad \beta_y = \beta_0\left(1 + \frac{f_{\mathrm{or},1}}{2}\right) \tag{46}$$

2. Biaxial orientation

$$\alpha_x^a = \alpha_0(1 - f_{\mathrm{or},1}^a), \quad \alpha_y^a = \alpha_0(1 - f_{\mathrm{or},2}^a) \tag{47}$$

$$\alpha_x^c = \alpha_0(1 - f_c), \quad \alpha_y^c = \alpha_0(1 - f_c) \tag{48}$$

$$\beta_x = \beta_0(1 - f_{\mathrm{or},1}), \quad \beta_y = \beta_0(1 - f_{\mathrm{or},2}) \tag{49}$$

Anisotropic shrinkage in injection moldings

The volumetric shrinkage is predicted based on the specific volume, V, history which a polymeric melt passes through during the injection molding process. The volumetric shrinkage is calculated as[23]

$$S_V = \frac{\overline{V}_i - V_f}{\overline{V}_i} \tag{50}$$

where $\overline{V}_i$ is the initial specific volume of melt and $\overline{V}_f$ is the final specific volume at room temperature. Since the polymer melt undergoes severe pressure and temperature changes in a short time, the initial specific volume cannot be assumed to be as that at constant pressure and temperature conditions.[23,43] In the present simulation, the initial specific volume is calculated as[23]

$$\overline{V}_i = \frac{1}{(t_p - t_f)} \int_{t_f}^{t_p} \overline{V}(t)dt \tag{51}$$

where t_f is the filling time, t_p is the packing time, and $\overline{V}(t)$ is the time-dependent specific volume averaged through the gapwise direction for a particular cross section such that

$$\overline{V}(t) = \frac{1}{b} \int_0^b V(z,t)dz \tag{52}$$

The specific volume for semicrystalline polymers is calculated from Spencer-Gilmore equation of state[44] and represented as[38]

$$V(T,P) = \frac{1}{\rho(T,P)} = \frac{1}{\overline{\rho}} + \frac{\overline{R}}{P + \overline{P}} T + \frac{1}{\overline{\rho}_t} \tag{53}$$

if $T \geq T_t$

$$\frac{1}{\overline{\rho}_t} = b_7 \exp(b_8 \overline{T} - b_9 P), \quad \overline{\rho} = \overline{\rho}_l, \quad \overline{R} = \overline{R}_l, \quad \overline{P} = \overline{P}_l \tag{54}$$

if $T \leq T_t$

$$\frac{1}{\overline{\rho}_t} = 0, \quad \overline{\rho} = \overline{\rho}_x, \quad \overline{R} = \overline{R}_s, \quad \overline{P} = \overline{P}_s \tag{55}$$

with the transition temperature (crystallization temperature), $T_t = b_5 + b_6 P$, and $\overline{T} = T - b_5$.

Where b_5, b_6, b_7, b_8, b_9 and $\overline{\rho}_l$, $\overline{R}_l$, $\overline{P}_l$ and $\overline{\rho}_s$, $\overline{R}_s$, $\overline{P}_s$ are the material parameters obtained by fitting of eq. (53) to the specific volume data measured above and below the crystallization temperature for semicrystalline polymers.

The shrinkage changes in the injection molded products are determined by two effects: shrinkage due to cooling effects and shrinkage due to pressure effects. The cooling effect causes all layers to experience the same thermal contraction after ejection. In addition to this, each cross section solidifies under the different pressure and therefore, at the end of the packing stage, tends to expand proportional to the solidification pressure. By these two effects, the total shrinkage can be calculated by[27–30]

$$S_i = \alpha_i(T_s - T_\infty) - \beta_i \overline{P}_s, \quad i = x, y \tag{56}$$

where T_s is the solidification temperature, T_∞ is the ambient final temperature, and $\overline{P}_s$ is the average solidification pressure at each cross section which is calculated as[23]

$$\overline{P}_s(x) = \frac{1}{(t_{p0} - t_f)} \int_{t_f}^{t_{p0}} P(x,t)dt \tag{57}$$

or[29]

$$\overline{P}_s(x) = \frac{1}{b} \int_0^b P_s(x,z)dz \tag{58}$$

where t_{p0} is the time at which the pressure goes to zero and $P_s(x, z)$ is the pressure when the local temperature at each z reaches T_s (T_m for semicrystalline polymers).

When the temperature of polymer melt reaches to the elevated melting temperature, T_m, crystallization starts to take place. At that time, a recoverable elastic strain, introduced during flow, in the both crystalline and amorphous regions should be frozen-in due to crystallization. However, the recoverable strain in the amorphous region can relax until the glass transition temperature is achieved. At the end of packing stage, a recovery of elastic strain in the amorphous region occurs due to abrupt pressure decay caused by release

TABLE I
Material Specification and Model Parameters for PET, PBT, and PEN

	PET	PBT	PEN
Material specification			
I. V. (dl/g)	0.74	1.24	0.64
Thermal properties			
k (W/mK)	0.29[7]	0.175[45]	0.23[45]
C_p (10^{-3} J/kg K)	1.13[46]	2.140[45]	2.165[45]
ρ (kg/m^3)	1330[46]	1110[45]	1166[45]
Crystallization model parameters			
$(1/t_{1/2})_0 \times 10^{-6}$ (s^{-1})	0.0358[7]	0.0338	0.000894
$K_k \times 10^{-5}$ (K^2)	3.66[7]	2.68	1.98
n	2.1[7]	3.0	3.0
ΔH_m^0 (J/g)	26.9[46]	32.0[46]	25.0[46]
X_∞	0.32[7]	0.45	0.42
f_{cr}	0.006	0.0012	0.006
T_m^0 (°C)	280[47]	245[46]	270[47]
T_g (°C)	80[46]	55[46]	110[46]
κ	74.97[43]		
Rheological model parameters			
s	0.001	0.001	0.001
T_b (K)	14,817	28,985	10,033
A_1 (Pa s)	1.403 e −10	1.717 e −21	1.512 e −6
A_2 (Pa s)	7.001 e −11	7.680 e −22	5.455 e −6
A_3 (Pa s)	1.389 e −10	2.938 e −22	6.087 e −6
B_1 (s)	1.844 e −14	2.794 e −26	5.001 e −10
B_2 (s)	1.845 e −15	2.785 e −27	4.968 e −11
B_3 (s)	1.846 e −16	2.775 e −28	4.936 e −12

of the packing pressure. This elastic recovery contributes to the total shrinkage causing abrupt planar dimension change at the time of end of packing. The elastic recovery contribution to the total shrinkage for semicrystalline polymers is calculated based on the amorphous contribution of the total elastic recovery accumulated until the elevated melting temperature:

$$S_{\gamma_\infty} = (1 - \chi_p) \int_0^{t_{Tm}} \dot{\gamma}_e(t) dt \tag{59}$$

where χ_p is the absolute crystallinity at the time of end of packing and t_{T_m} is the time when the elevated melting temperature is reached.

Without affecting volumetric shrinkage, this elastic recovery can be applied to the length and width shrinkages only, due to freezing of extensive skin layer that causes geometric constraints that prevents the thickness shrinkage during the packing stage. Because of heat transfer inside the mold cavity, the wall region is already solidified, while the core region is still remained in melt state due to slow cooling rate in this region. This solidified wall region acts as a constraint, not allowing a further shrinkage in the thickness direction. Therefore, the unfrozen elastic recovery at the end of packing stage can be applied to cause a shrinkage in the length direction and simultaneously applied to cause an expansion in the width direction. At this moment, the thickness shrinkage remains constant. This way, the volumetric shrinkage is preserved.

Therefore, the final length and width shrinkages are calculated by considering the amorphous and crystalline contribution to the total thermal contraction, separately, as

$$S_x = (1 - \chi)\alpha_x^a (T_g - T_\infty) + \chi \alpha_x^c (T_m - T_\infty) - \beta_x \overline{P}_s + S_{\gamma_\infty} \tag{60}$$

TABLE II
Optical Properties and Material Constants in the Spencer–Gilmore *P–V–T* Equation of State for PET, PBT, and PEN

	PET	PBT	PEN
Spencer–Gilmore equation:			
$T \geq T_t$			
$\overline{\rho}_l$ (kg/m^3)	1.961 e +3	1.818 e +3	1.531 e +3
$\overline{R}_l$ (J/kg K)	2.360 e +2	2.687 e +2	8.873 e +2
$\overline{P}_l$ (Pa)	4.902 e +8	5.638 e +8	2.569 e +9
$T < T_t$			
$\overline{\rho}_s$ (kg/m^3)	1.706 e +3	1.590 e +3	1.476 e +3
$\overline{R}_s$ (J/kg K)	1.319 e +2	1.559 e +2	1.109 e +2
$\overline{P}_s$ (Pa)	5.621 e +8	4.733 e +8	6.414 e +8
b_5 (K)	5.054 e +2	4.873 e +2	5.442 e +2
b_6 (K/Pa)	1.630 e −7	1.440 e −7	1.640 e −7
b_7 (m^3/kg)	5.730 e −5	6.330 e −5	6.703 e −5
b_8 (K^{-1})	5.693 e −2	5.218 e −2	3.677 e −2
b_9 (kg/m^3)	1.140 e −6	1.030 e −8	7.604 e −9
Δn_a^0	0.275[48]	0.210[49]	0.504[50]
Δn_c^0	0.290[51]	0.153[52]	0.463[50]
C (Pa^{-1})	7.8 e −9[48]	2.0 e −8[53,54]	2.75 e −8[55]
$\alpha_0 \times 10^{-4}$ (K^{-1})	1.2404[46]	1.4318	0.832
$\beta_0 \times 10^{-5}$ (Pa^{-1})	0.0667[46]	0.0473	–

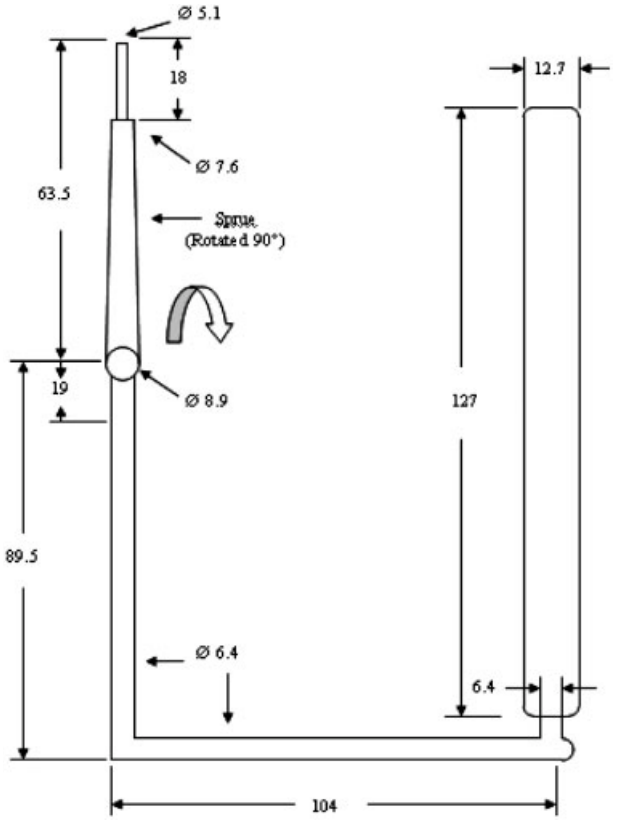

Figure 1 Dimensions of mold, runner system and sprue for Charpy impact bar mold. Cross section of the melt delivery system is circular. Cross section of the gate and cavity is rectangular (unit: mm). Thickness of cavity and gate: 3.175 mm.

$$S_y = (1-\chi)\alpha_y^a(T_s - T_\infty) + \chi\alpha_y^c(T_m - T_\infty) - \beta_y\overline{P}_s - S_{\gamma_\infty} \quad (61)$$

From the calculated length and width shrinkage, the thickness shrinkage is calculated as

$$S_z \cong S_v - (S_x + S_y) \quad (62)$$

EXPERIMENTAL

Materials and injection moldings

In this study, PET, PBT, and PEN were used for slow-crystallizing polymers. PET, Eastapak PET Polyester 7352, was provided by Eastman Chemical Company and PEN, VFR-40046, was supplied by Shell Chemical Company. PBT, Ultradur KR 4036-Q692, was provided by BASF AG. The thermal properties and the intrinsic viscosity are listed in Table I.

The PVT material parameters are obtained by fitting the experimental data to Spencer-Gilmore equation, eqs. (53)–(55). The experimental data of specific volume at different pressures for PET, PBT, and PEN were obtained from C-Mold database.[45] The obtained PVT material parameters and optical properties are listed in Table II. The isotropic thermal expansion and compressibility for PBT and PEN are obtained from the PVT behavior.

The injection molding experiments were carried out on Van Dorn 50 screw injection molding machine. An ASTM Charpy impact bar cavity shown in Figure 1 was used to measure the anisotropic shrinkage. The injection molding experiments were carried out for PET and PBT under different processing conditions with varying packing pressure (P_p), packing time (t_p), flow rate (Q), melt temperature (T_0) and mold temperature (T_w) as shown in Tables III and IV. For PEN, the injection molding experiments were carried out under different packing pressure and packing time and the conditions are shown in Table V.

Quiescent crystallization

The model parameters for the quiescent crystallization kinetics were obtained for PET 7352 by Chan and Isayev.[7] To obtain the model parameters of the crystallization kinetics for PBT and PEN, the isothermal and nonisothermal experiments were carried out by using

TABLE III
Processing Conditions for Injection Molding Process of Charpy Impact Bars of PET 7352[a]

	Packing pressure (MPa)	Packing time (s)	Flow rate (cm^3/s)	Melt temp. (°C)	Mold temp. (°C)
1	34.5	5	35.9	300	60
2	20.67	5	35.9	300	60
3	68.9	5	35.9	300	60
4	34.5	2	35.9	300	60
5	34.5	10	35.9	300	60
6	34.5	15	35.9	300	60
7	34.5	5	8.95	300	60
8	34.5	5	107.4	300	60
9	34.5	5	35.9	280	60
10	34.5	5	35.9	320	60
11	34.5	5	35.9	300	110

[a] Cooling time: 30 s.

TABLE IV
Processing Conditions for Injection Molding Process of Charpy Impact Bars of PBT[a]

	Packing pressure (MPa)	Packing time (s)	Flow rate (cm^3/s)	Melt temp. (°C)	Mold temp. (°C)
1	34.5	5	35.9	280	60
2	20.67	5	35.9	280	60
3	68.9	5	35.9	280	60
4	34.5	2	35.9	280	60
5	34.5	10	35.9	280	60
6	34.5	15	35.9	280	60
7	34.5	5	8.95	280	60
8	34.5	5	107.4	280	60
9	34.5	5	35.9	260	60
10	34.5	5	35.9	300	60
11	34.5	5	35.9	280	110

[a] Cooling time: 30 s.

TA DSC (DSC-Q1000).[56] The obtained nonisothermal crystallization rate constants for PBT and PEN are shown in Figure 2 with the calculated crystallization rate constants for PET[7] and PP 6523.[57] By fitting the Hoffman-Lauritzen equation to the experimental data, model parameters for the crystallization kinetics, $(t_{1/2})_0^{-1}$ and K_k, are obtained and listed in Table I.

Rheological model parameters

Figures 3–5 show the flow curves at three different temperatures for PET, PBT and PEN. The experimental data for PET, PBT and PEN used in this study were measured by Song.[58] By fitting the nonlinear constitutive equation, eqs. (8) and (24), the model parameters of three relaxation modes are obtained and listed in Table I.

Birefringence and shrinkage measurement

To measure the birefringence of injection molded samples, optical microscope of Leitz Laborlux 12 POL S was used with 4th order compensator (Leitz Laborlux). The specimens of 10 mm thickness were prepared by cutting at the midway of a molded sample by using diamond saw (Buehler Isomet). Then, the cut sample was cut parallel to x–z plane by a diamond saw to thickness of 500 μm. Birefringence was determined by measuring the phase difference (retardation) through a sample as

$$\Delta n = \frac{\Gamma}{d} \tag{63}$$

where Γ is the retardation and d is the sample thickness.

The shrinkage in the three different directions, i.e., the length, width and thickness directions of the Charpy impact bar was measured using a digital micrometer (Mitutoyo Digimatic) for the length and width directions, and a digital micrometer (Monsanto) for the thickness direction. The part dimensions are divided by the mold dimensions to calculate the percent shrinkage. The thickness and width shrinkages are measured at three different distances located at 22, 63.5, and 103 mm from the gate and their averaged value was used for comparison with the corresponding simulated data. The overall length of moldings was measured to calculate the length shrinkage and its value was used for comparison with the corresponding value obtained from simulation.

Meshes and numerical scheme

The numerical simulations of the injection molding process of slow crystallizing polymers were carried out by the finite difference method using ANSI C pro-

TABLE V
Processing Conditions for Injection Molding Process of Charpy Impact Bars of PEN[a]

	Packing pressure (MPa)	Packing time (s)	Flow rate (cm^3/s)	Melt temp. (°C)	Mold temp. (°C)
1	34.5	5	35.9	300	60
2	20.67	5	35.9	300	60
3	68.9	5	35.9	300	60
4	34.5	2	35.9	300	60
5	34.5	10	35.9	300	60
6	34.5	15	35.9	300	60

[a] Cooling time: 30 s.

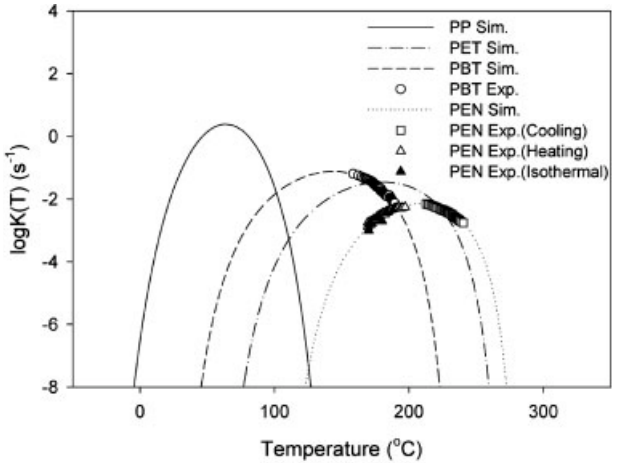

Figure 2 The measured (symbols) and predicted (lines) nonisothermal crystallization rate constants for PET,[7] PBT, and PEN under the quiescent crystallization. Two isothermal data points for PEN and the predicted nonisothermal data for PP 6523[57] were added.

gramming language. The mesh was generated over the charpy impact bar mold cavity and the delivery system, which were divided into 12 segments and equally spaced 182 nodes in the flow direction. The half thickness in the delivery system and the cavity was discretized into equally-spaced 65 nodes.

In the filling stage, the temperature at the sprue entrance is assumed to be uniform and equal to the inlet melt temperature, T_0. First, the flow at the melt front is assumed to be the fully developed Poiseuille-type. The melt front, X_f, progresses regularly one space of Δx at the time step of Δt, starting from the sprue entrance to the end of cavity. The initial guess for the shear rate are given by[35]

$$\dot{\gamma}(x_f, z_j, 0) = \frac{3\overline{v}_x}{b^2} z_j \text{ (Cartesian coordinate)} \qquad (64)$$

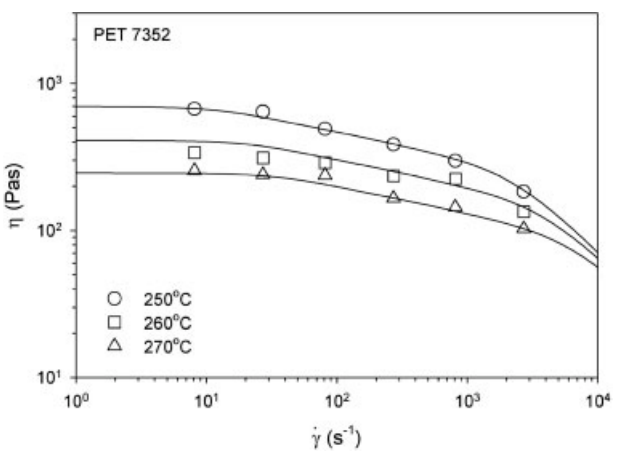

Figure 3 Flow curves at various melt temperatures as a function of shear rates for PET 7352. Symbols represent the experimental data[58] while lines indicate the nonlinear regression fit to eqs. (8) and (24).

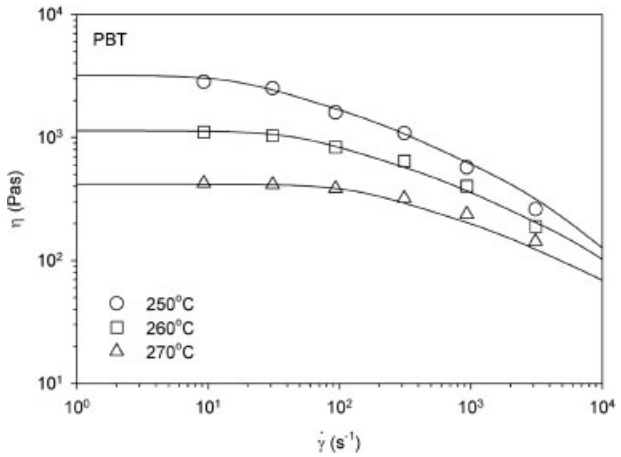

Figure 4 Flow curves at various melt temperatures as a function of shear rates for PBT. Symbols represent the experimental data[58] while lines indicate the nonlinear regression fit to eqs. (8) and (24).

$$\dot{\gamma}(x_f, z_j, 0) = \frac{4\overline{v}_x}{b^2} z_j \text{ (cylindrical coordinate)} \qquad (65)$$

During the filling stage, the elastic strain tensor, $C_{ij,k}(x_f,z_j,t)$, is calculated by using the steady state formulations, eqs. (21)–(23) and satisfying the shear rate and pressure gradient, eqs. (18) and (20). Then, the shear rates, $\dot{\gamma}(x_f, z_j, t)$, is obtained by solving eqs. (18) and (20)–(23) by means of the Newton-Raphson iterative method.[59] The melt front moves along the flow direction until it reaches the end of the cavity.

In the packing stage, an additional melt is injected into the mold cavity to compensate the specific volume change due to cooling. The flow rate as a function of time during the packing stage is calculated based on the volume change between the mold cavity and

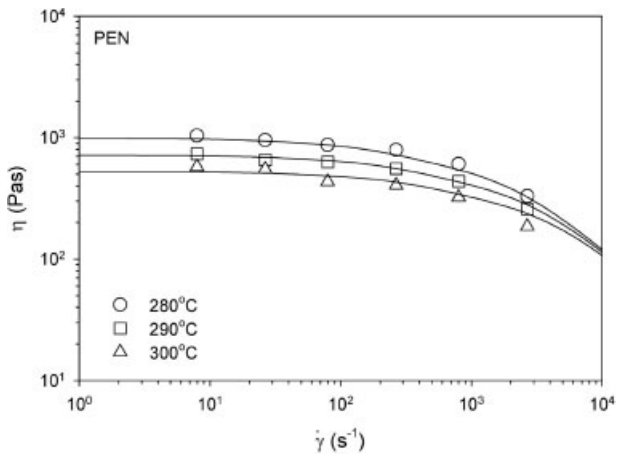

Figure 5 Flow curves at various melt temperatures as a function of shear rates for PEN. Symbols represent the experimental data[58] while lines indicate the nonlinear regression fit to eqs. (8) and (24).

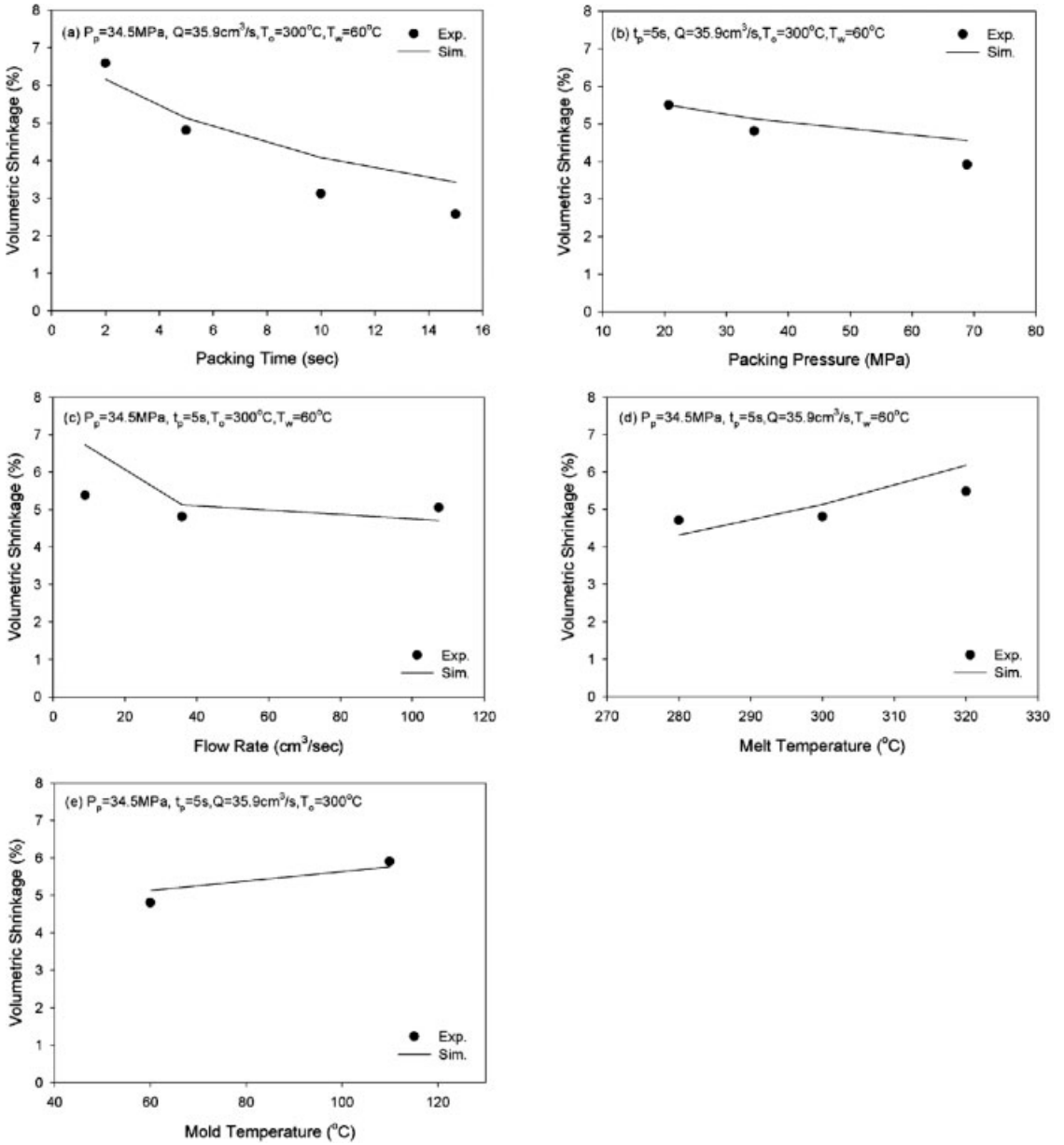

Figure 6 The measured (symbols) and predicted (lines) volumetric shrinkage for PET as a function of packing time (a), packing pressure (b), flow rate (c), melt temperature (d) and mold temperature (e).

the material in the cavity at current temperatures and pressures.

During the filling and packing stage, the transient process takes place very fast. This is due to the very small relaxation time for slow crystallizing polymers as indicated by model parameters in Table I. Therefore, a steady state calculation for all three modes was used for elastic strain tensor and shear rate.

In the cooling stage, the flow is ceased and therefore, the velocity and shear rates are set to zero. The flow stresses developed during the filling and packing stages start to relax. To consider the relaxation behavior, the transient calculations were used based on eqs. (15)–(17) since the relaxation times are increased by temperature decrease.

RESULTS AND DISCUSSION

Volumetric shrinkage

Figures 6 and 7 show the measured and calculated volumetric shrinkage in moldings of Charpy impact bar of PET and PBT, respectively, as a function of packing time (a), packing pressure (b), flow rate (c), melt temperature (d), and mold temperature (e). Figure 8 illustrates the measured and predicted volumetric shrinkage of PEN in Charpy impact bar as a function of pack-

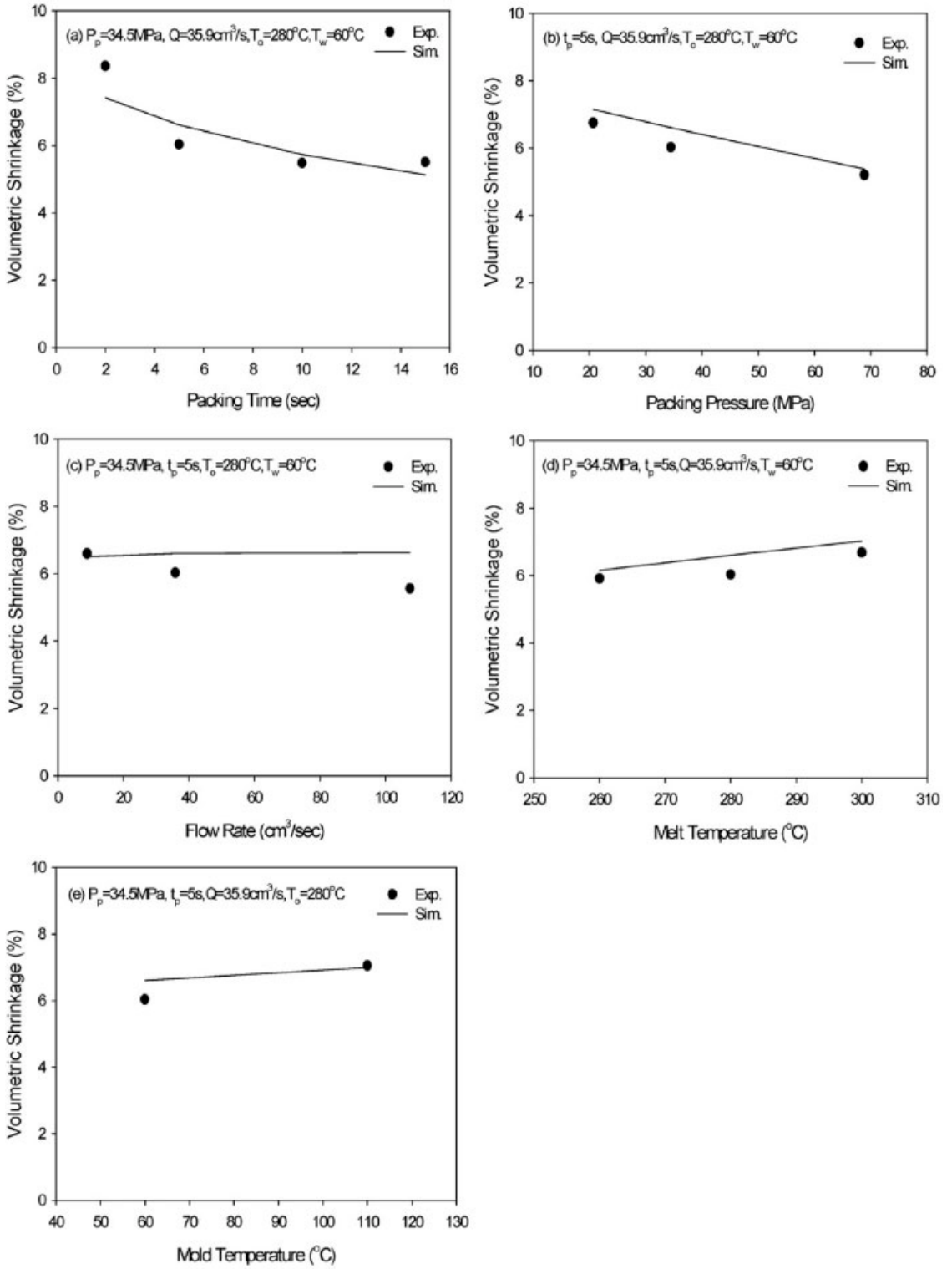

Figure 7 The measured (symbols) and predicted (lines) volumetric shrinkage for PBT as a function of packing time (a), packing pressure (b), flow rate (c), melt temperature (d) and mold temperature (e).

ing time (a) and packing pressure (b). To calculate the variation of specific volume and resulting volumetric shrinkage during molding process, the material parameters of Spencer-Gilmore equation shown in Table II, were used.

For all cases, as the packing time increased, the volumetric shrinkage decreased, as shown in Figures 6(a), 7(a), and 8(a). Similarly, both measured and calculated volumetric shrinkage decreased as the packing pressure increased, as indicated in Figures 6(b), 7(b), and

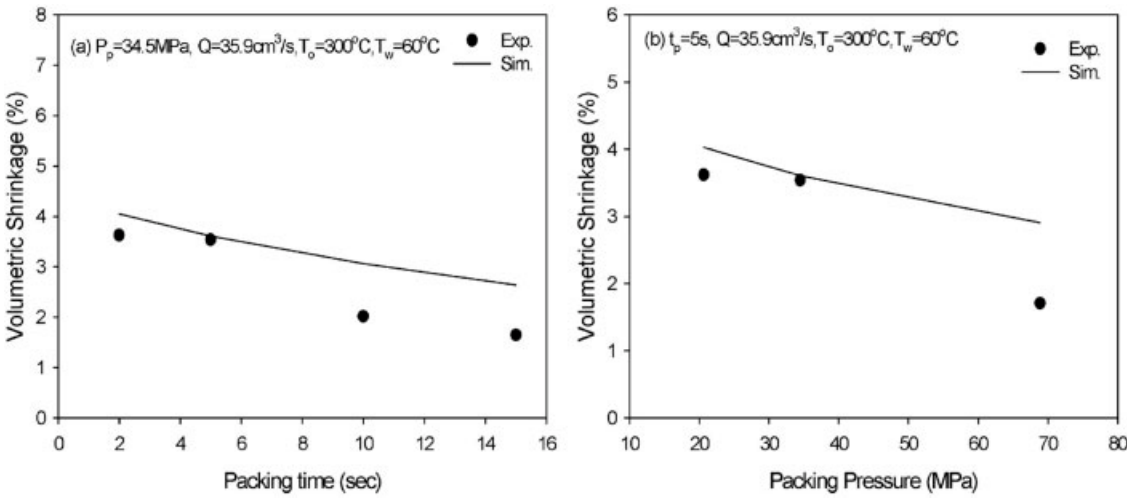

Figure 8 The measured (symbols) and predicted (lines) volumetric shrinkage for PEN as a function of packing time (a) and packing pressure (b).

8(b). This was due to the fact that, at longer packing time or higher packing pressure, more material was injected into the cavity to compensate for the shrinkage due to cooling. The predicted volumetric shrinkage in PET, PBT, and PEN showed a fair agreement with the experimental data even at the longer packing time and higher packing pressure. This is in contrast to shrinkage data obtained for amorphous polystyrene[33] showing at longer packing time, the simulations deviates from the experimental data. The deviation was explained as a result of gate freezing effect. It was due to the fact that the effect of gate freezing was not as significant as in case of PS. In slow crystallizing polymers, such as PET, PBT, and PEN, gate freezing effect took place relatively slowly due to the very high inlet melt temperature, T_0, and therefore relatively larger difference between T_0 and mold temperature, T_g. Therefore, the effect of packing pressure was more dominant for slow crystallizing polymers than in PS.

With the variation of flow rate, both measured and predicted volumetric shrinkage did not show much difference as indicated in Figures 6(c) and 7(c). The effect of the melt and mold temperature on volumetric shrinkage was shown in Figures 6(d) and 6(e) and 7(d) and (e) for PET and PBT. As the melt and mold temperature increased, the volumetric shrinkage increased due to the higher thermal contraction and increased contribution of cooling effect while molding cooled to the room temperature. Similar behaviors of shrinkage were observed for amorphous (PS)[33] and fast crystallizing polymers (PP).[34] For PET molded samples, similar experimental results were shown[43] about the effect of packing pressure and mold temperature, as a higher packing pressure and lower mold temperature gave lower volumetric shrinkage. However, in case of the melt temperature, in contrast to observation of our study, an opposite trend of volumetric shrinkage was observed in,[43] namely, the volumetric shrinkage decreased with increasing melt temperature. Generally, the larger shrinkage obtained at higher melt temperature is due to the larger volume contraction associated with a larger difference between melt and mold temperature. However, simultaneously, the viscosity is decreased at higher melt temperature and more material can be injected into the cavity during packing stage. This additional material can offset the contraction in volume due to cooling and the volumetric shrinkage would decrease with increasing melt temperature. Therefore, in the present study, the volume contraction effect was more dominant than the viscosity effect.

Figure 9 shows the comparisons of measured and predicted volumetric shrinkages in various polyesters as a function of packing time (a) and packing pressure (b). For PEN, the observed shrinkages in both experiments and simulations were much smaller than those of PET and PBT. In fact, the obtained value of shrinkage seems to be clearly related to the crystallization rate of each polymer as shown in Figure 2. The PBT showing the highest crystallization rate showed the highest volumetric shrinkage in both measurements and calculations, while PEN with the lowest crystallization rate showed the lowest volumetric shrinkage among various polymers.

Birefringence and anisotropic shrinkage

To predict anisotropic shrinkage in molded products, the orientation functions based on the different assumption discussed in theoretical section are considered. Figure 10 shows the gapwise distribution of measured and predicted birefringence at midway of PET molded sample. The birefringence is mainly developed near the wall region because of high shear rate

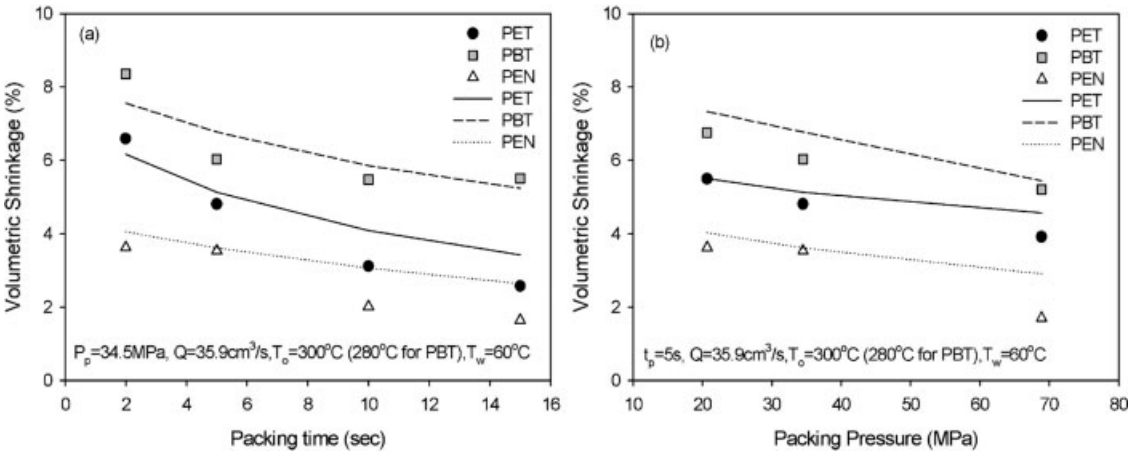

Figure 9 The measured (symbols) and predicted (lines) volumetric shrinkage of PET, PBT, and PEN as a function of packing time (a) and packing pressure (b).

and fast cooling in this region. Typically, during packing stage, the birefringence starts to develop in the core region due to additional packing flow. However, for PET samples, since the glass transition temperature is higher than the room temperature and reaches at very early stage of packing, the flow birefringence in the core region cannot be developed. The existence of birefringence in the core region seen in Figure 10 is due to the frozen-in thermal birefringence which was not considered in the present study. By comparison, the predicted flow birefringence based on this approach is found to be in fair agreement with the experimental data.

On the basis of the different orientation assumption, the thermal expansion coefficient and compressibility were calculated as a function of uniaxial [eqs. (44)–(46)] and biaxial [eqs. (47)–(49)] orientation functions. For slow crystallizing polymers, the amorphous and crystalline regions are frozen at different temperature, T_g and T_m, respectively. Therefore, the amorphous and crystalline contribution to the total thermal contraction was separately considered as indicated in eqs. (60) and (61).

The measured anisotropic in-plane shrinkages were compared with the predicted ones that were calculated using different orientation assumptions as shown in Figure 11 for the uniaxial (a), (c) and biaxial (b), (d) orientations. With the variation of packing time and packing pressure, the predicted length and width shrinkage did not show much difference by using the different orientation assumptions. This is possibly due to the fact that the developed orientation during molding process is too small to distinguish the differences between the uniaxial and biaxial orientation assumptions. Therefore, further calculations were conducted based on the uniaxial orientation assumption. Calculations also showed that the anisotropic shrinkages are not affected by the way solidification pressure was calculated, i.e., use of eqs. (57) or (58).

The anisotropic shrinkages in the length, width and thickness directions were calculated as a function of processing conditions by using eqs. (60)–(62). The thermal contraction in the amorphous and crystalline region was independently considered due to the different freezing temperature of amorphous and crystalline phases. Calculations were carried out with inclusion of contribution of unfrozen elastic recovery, calculated from eq. (59). Comparisons between the measured and predicted results are shown in Figures 12–14 for PET, PBT, and PEN, respectively.

Figure 12 shows the measured and predicted anisotropic shrinkage of PET molded samples as a function of packing time (a), packing pressure (b), flow rate (c), melt temperature (d), and mold temperature (e). As the packing time increases, the shrinkage in the thickness direction decreases since the more material is injected to compensate for the volume contraction during cooling, while the predicted length and width shrinkages did not show much difference. With increasing packing pressure, the length and width

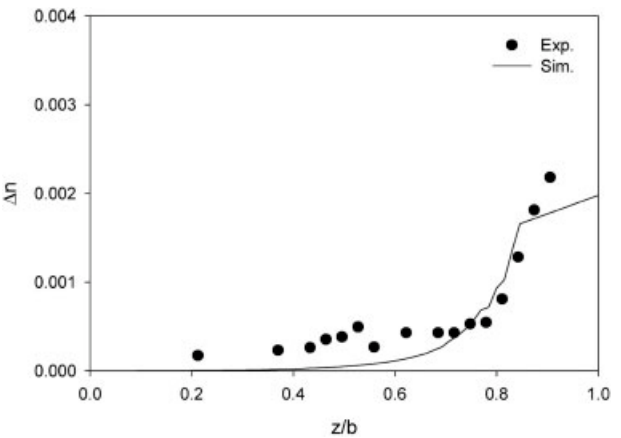

Figure 10 Gapwise distribution of measured (symbols) and calculated (line) birefringence of PET at midway of cavity. Processing conditions: $P_p = 34.5$ MPa, $t_p = 5$ s, $Q = 35.9$ cm^3/s, $T_0 = 300^\circ$C and $T_w = 60^\circ$C.

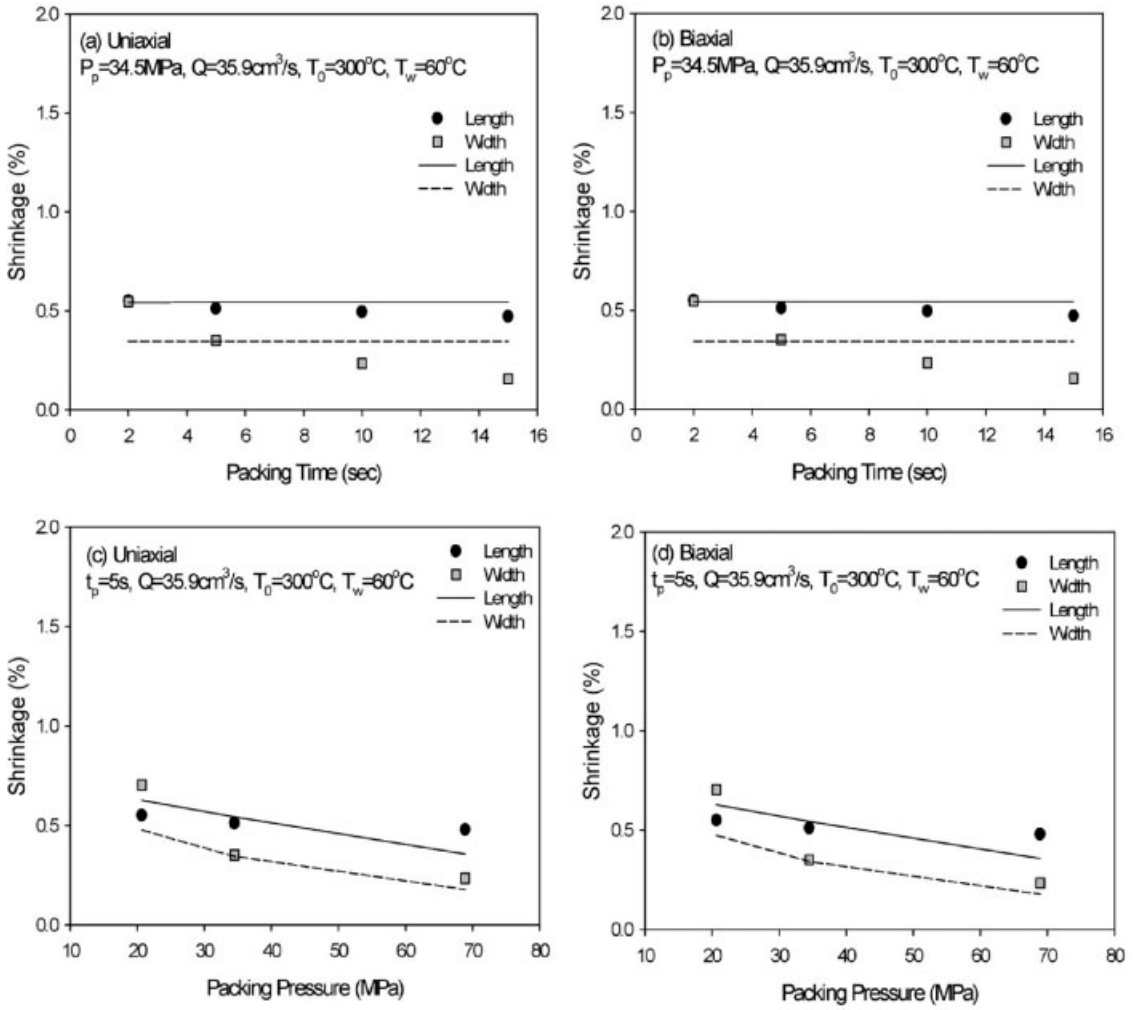

Figure 11 Measured (symbols) and predicted (lines) length and width shrinkages for PET as a function of packing time (a), (b) and packing pressure (c), (d) using assumption of uniaxial and biaxial orientation.

shrinkage as well as thickness shrinkage decrease. With the variation of flow rate (c), melt (d) and mold (e) temperature, the thickness shrinkage was slightly affected, while the length and width shrinkage did not show particular trend. The predicted values were found to be in a fair agreement with the experimental data. Among all shrinkages, the thickness shrinkage is always much higher than the in-plane shrinkage and the length shrinkage is slightly larger than the width shrinkage. The most important processing conditions to control the shrinkage of PET moldings were packing time and packing pressure. Among various anisotropic shrinkages, the thickness shrinkage was most strongly affected by the processing conditions.

Similar behavior of anisotropic shrinkage was observed in Figure 13 for PBT molded samples. The thickness shrinkage was mainly affected by the packing time and packing pressure. The length and with shrinkages showed little effect with the variation of processing conditions. For PBT, the difference between the length and width shrinkage was very small in both measured and predicted results. It was due to the fact that the elastic recovery developed in PBT melt during molding process is very small. This was caused by very small relaxation time and very large activation energy as indicated in Table I. Even though the difference between the length and width shrinkage was very small, the length shrinkage was slightly larger than the width shrinkage.

Figure 14 shows the measured and predicted anisotropic shrinkage for PEN molded samples as a function of packing time (a) and packing pressure (b). For PEN, due to its low crystallization rate, the crystallinity was not developed during molding. Therefore, the crystalline contribution to the anisotropic shrinkage does not exist. Accordingly, similar to the amorphous polymer (PS),[41] the compressibility effect was neglected since the PEN molded sample was almost amorphous. As the packing time and packing pressure increased, the thickness shrinkage decreased, while the length and width shrinkage showed little variation. The calculated thickness and length shrinkage showed a fair agree-

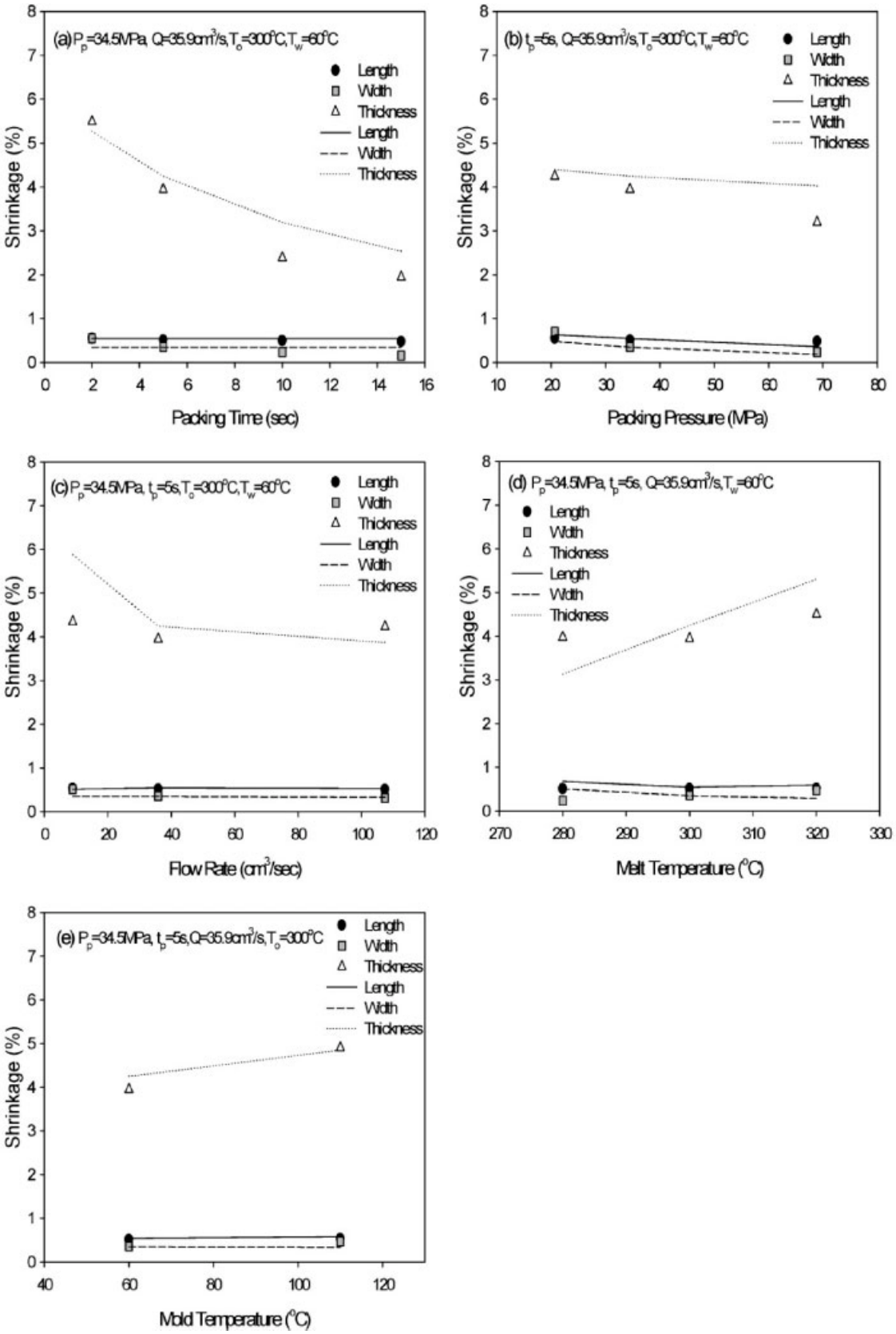

Figure 12 The measured (symbols) and predicted (lines) anisotropic shrinkage for PET as a function of packing time (a), packing pressure (b), flow rate (c), melt temperature (d) and mold temperature (e).

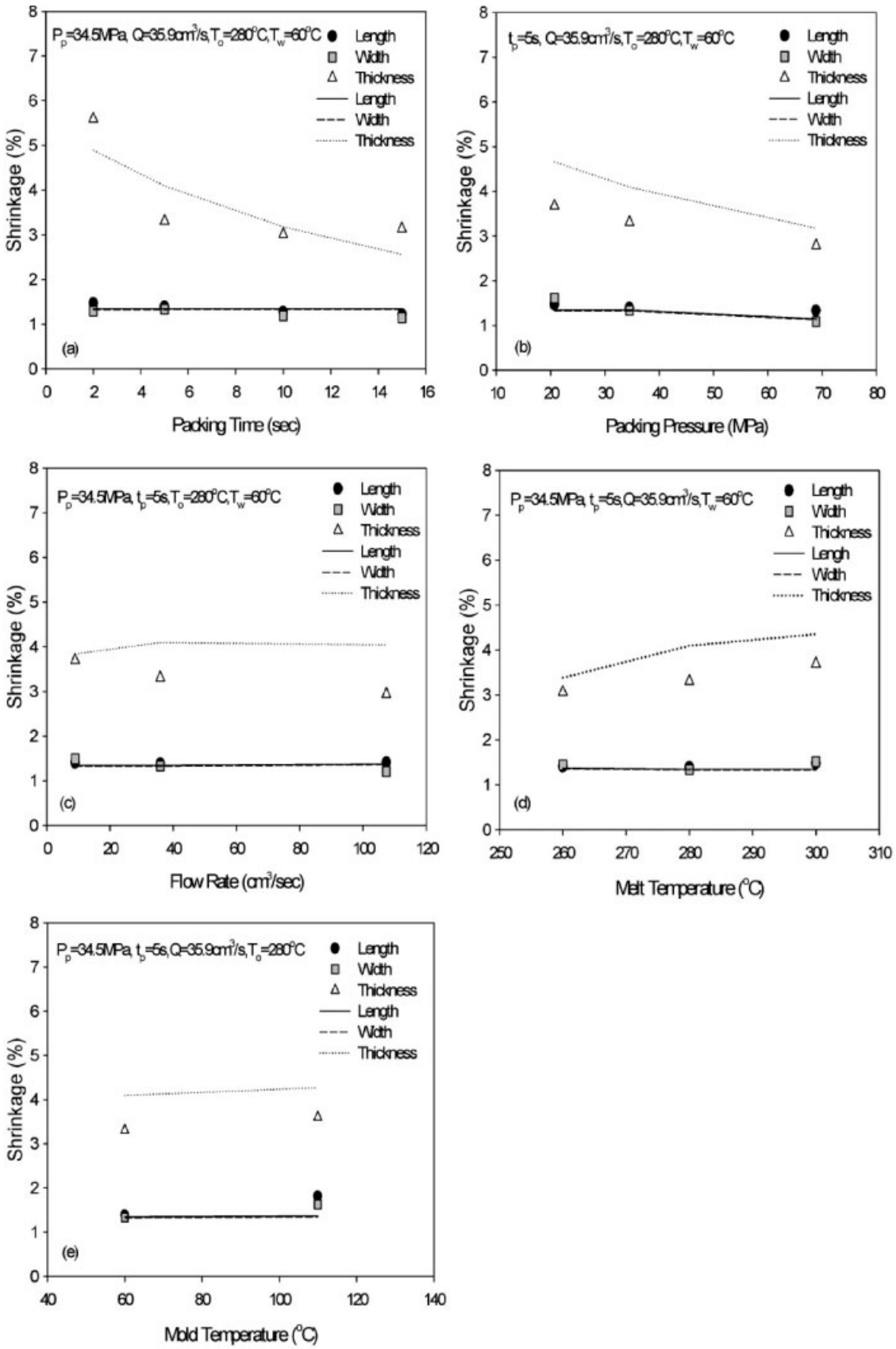

Figure 13 The measured (symbols) and predicted (lines) anisotropic shrinkage for PBT as a function of packing time (a), packing pressure (b), flow rate (c), melt temperature (d) and mold temperature (e).

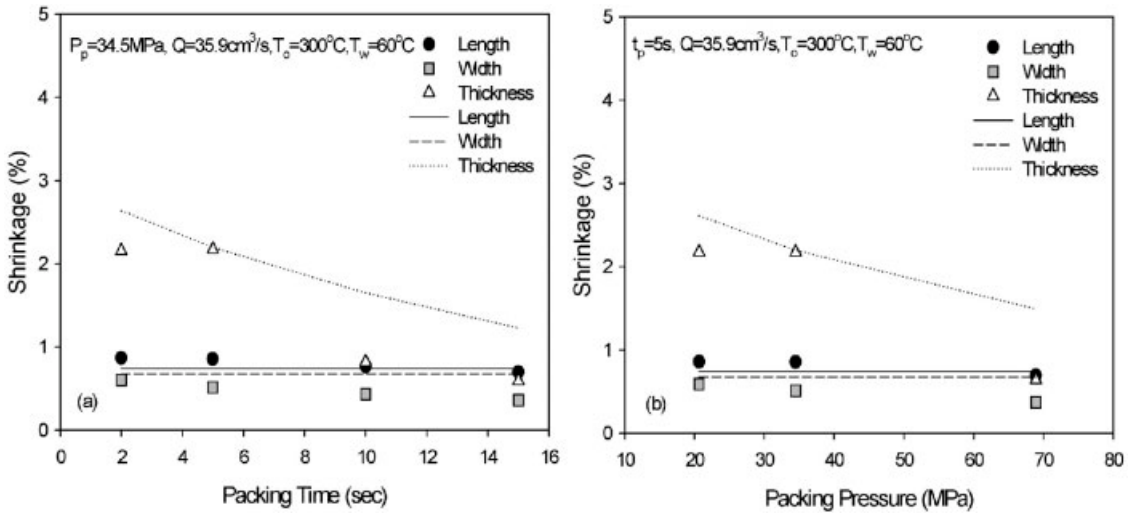

Figure 14 The measured (symbols) and predicted (lines) anisotropic shrinkage for PEN as a function of packing time (a) and packing pressure (b).

ment with the experimental data, while the calculated width shrinkage did not show decrease as indicated by the measured data with increasing packing time. This is possibly due to the fact that the heat transfer in the width direction is not included in this simulation.

Finally, it should be noted that among various anisotropic shrinkages for the three polyesters, the thickness shrinkage was most strongly affected by the processing conditions. Clearly, this is due to the fact that the heat transfer during molding process mostly occurs in the thickness direction leading to significant contraction in this direction during cooling. At the same time, the heat transfer in the flow and width directions is weak. Accordingly, the length and width shrinkages are less affected by the processing conditions.

CONCLUSIONS

A novel approach to predict anisotropic shrinkage in the injection-molded parts of slow crystallizing polymers was proposed based on the frozen-in orientation function and elastic recovery. The predicted results were compared with experimental data obtained at different processing conditions such as packing time, packing pressure, flow rate, melt temperature and mold temperature. To introduce anisotropy into in-plane shrinkage, anisotropic LTEC and compressibility as a function of orientation function were calculated. For slow crystallizing polymers, the developed crystallinity and rate of crystallization is very low and the glass transition temperature is higher than the room temperature. Therefore, since freezing of the amorphous and crystalline region in moldings of PET, PBT, and PEN take place at glass transition and at melting temperature, respectively, the thermal expansion coefficients contribution to shrinkage in each region was considered independently. The total frozen-in orientation function was calculated based on the amorphous contribution determined from flow birefringence through the stress-optical rule and the crystalline contribution determined from the crystalline orientation function obtained from the elastic recovery. The uniaxial and biaxial orientation assumptions were tested and their effect on the anisotropic in-plane shrinkage was investigated. To predict the experimentally observed difference between the length and width shrinkages, amorphous contribution of elastic recovery to the anisotropic shrinkage that was not frozen-in during the crystallization of melt was considered. In agreement with experiments, the predicted thickness shrinkage was much higher than the predicted length and width shrinkages. The length shrinkage was slightly higher than the width shrinkage. The packing time was found to be one of the most important parameter affecting the anisotropic shrinkage. The length and width shrinkage were hardly affected by various processing conditions. Among various polyesters, PBT showed the highest volumetric and also highest thickness, length and width shrinkages, while PEN showed the lowest volumetric and thickness shrinkage. This behavior is related with the crystallization rate of each polymer. All predicted anisotropic shrinkages were shown to be in a fair agreement with the experimental results.

References

1. Hoffman, I. D.; Davis, G. T.; Lauritzen, S. I. In Treatise on Solid State Chemistry, Vol. 3; Hannay, N. B., Ed.; Plenum: New York, 1976; Chapter 7.
2. Nakamura, K.; Watanabe, T.; Katayama, K.; Amano, T. J Appl Polym Sci 1972, 16, 1077.
3. Nakamura, K.; Katayama, K.; Amano, T. J Appl Polym Sci 1973, 17, 1031.
4. Schneider, W.; Koeppl, A.; Berger, J. Int Polym Proc 1988, 2, 151.

5. Avrami, M. J Chem Phys 1939, 7, 1103.
6. Kolmogoroff, A. N. Isvestiya Akad Nauk SSSR, Ser Math 1937, 1, 355.
7. Chan, T. W.; Isayev, A. I. Polym Eng Sci 1994, 34, 461.
8. Chan, T. V.; Shyu, G. D.; Isayev, A. I. Polym Eng Sci 1995, 35, 733.
9. Flory, P. J. J Chem Phys 1947, 15, 397.
10. Dunning, W. J. Trans Faraday Soc 1954, 50, 1115.
11. Krigbaum, W. R.; Roe, R. J. J Polym Sci 1964, 2, 4391.
12. Haas, T. W.; Maxwell, B. Polym Eng Sci 1969, 9, 225.
13. Gaylord, R. J. J Polym Sci Polym Phys Ed 1976, 14, 1827.
14. Isayev, A. I.; Chan, T. W.; Shimojo, K.; Gmerek, M. J Appl Polym Sci 1995, 55, 807.
15. Isayev, A. I.; Chan, T. W.; Gmerek, M.; Shimojo, K. J Appl Polym Sci 1995, 55, 821.
16. Guo, X.; Isayev, A. I.; Guo, L. Polym Eng Sci 1999, 39, 2096.
17. Guo, X.; Isayev, A. I.; Demiray, M. Polym Eng Sci 1999, 39, 2132.
18. Palluch, K. P.; Isayev, A. I. Proceedings of the 13th International Congress on Rheology, Cambridge, UK, 2000; Vol. 2, pp 94–96.
19. Kim, K. H.; Isayev, A. I.; Kwon, K. SPE ANTEC 2003, 49, 713.
20. Kim, K. H.; Isayev, A. I.; Kwon, K. J Appl Polym Sci 2005, 95, 502.
21. Kim, K. H.; Isayev, A. I.; Kwon, K.; van Sweden, C. Polymer, 2005, 46, 4183.
22. Hellmeyer, H. O.; Menges, G. SPE ANTEC 1976, 22, 386.
23. Isayev, A. I.; Hariharan, T. Polym Eng Sci 1985, 25, 271.
24. Chiang, H. H.; Himasekhar, K.; Santhanam, N.; Wang, K. K. J Eng Mater Tech, Trans ASME 1993, 115, 37.
25. Bushko, W. C.; Stokes, V. K. Polym Eng Sci 1995, 35, 351.
26. Bushko, W. C.; Stokes, V. K. Polym Eng Sci 1995, 35, 365.
27. Jansen, K. M. B.; Titomanlio, G. Polym Eng Sci 1996, 36, 2029.
28. Titomanlio, G.; Jansen, K. M. B. Polym Eng Sci 1996, 36, 2041.
29. Jansen, K. M. B.; Pantani, R.; Titomanlio, G. Polym Eng Sci 1998, 38, 254.
30. Jansen, K. M. B. Int Polym Proc 1998, 13, 309.
31. Hieber, C. A. Polym Eng Sci 2002, 42, 1387.
32. Kennedy, P.; Zheng, R. SPE ANTEC 2003, 49, 593.
33. Kwon, K.; Isayev, A. I.; Kim, K. H. J Appl Polym Sci 2005, 98, 2300.
34. Kwon, K.; Isayev, A. I.; Kim, K. H.; van Sweden, C. SPE ANTEC, 2005, 51, 506.
35. Isayev, A. I.; Hieber, C. A. Rheol Acta 1980, 19, 168.
36. Leonov, A. I. Rheol Acta 1976, 15, 85.
37. Sobhanie, M.; Isayev, A. I. Rubber Chem Technol 1989, 62, 939.
38. Isayev, A. I., Ed. Injection and Compression Molding Fundamentals; Marcel Dekker: New York; 1987; Chapter 1.
39. Upadhyay, R. K.; Isayev, A. I.; Shen, S. F. Rheol Acta 1981, 20, 443.
40. Treloar, L. R. G. The Physics of Rubber Elasticity, 2nd ed.; Clarendon: Oxford, 1958; 342 pp.
41. Hennig, J. J Polym Sci Part C: Polym Symp, 1967, 16, 2751.
42. Choy, C. L.; Chen, F. C.; Ong, E. L. Polymer 1979, 20, 1191.
43. Han, S.; Wang, K. K. Int Polym Proc 1997, 12, 228.
44. Spencer, R. S.; Gilmore, G. D. J Appl Phys 1949, 20, 502.
45. C-MOLD Material Properties–Version 4.0, 1998.
46. Van Krevelen, D. W. Properties of Polymers, 3rd ed.; Elsevier: Amsterdam, 1990.
47. Brandrup, J.; Immergut, E. H. Polymer Handbook, 4th Ed.; Wiley-Interscience: New York, 1989.
48. Ziabicki, A. Fundamentals of Fiber Formation: The Science of Fiber Spinning and Drawing; Wiley: New York, 1976.
49. Gupta, V. B.; Ramesh, C. Polym Commun 1987, 28, 43.
50. Mitsuishi, M.; Ito, S.; Yammamoto, M.; Endo, H.; Hachiya, S.; Fischer, T.; Knoll, W. Macromolecules 1998, 31, 1565.
51. Ohkoshi, Y.; Nagura, M. Seni Gakkaishi 1993, 49, 601.
52. Ohkoshi, Y.; Okuya, T.; Nagura, M.; Konda, A. Seni Gakkaishi 1995, 51, 484.
53. Chen, S.; Yu, W.; Spruiell, J. E. J Appl Polym Sci 1987, 34, 1477.
54. Kim, K. J.; Kim, S. H. J Korean Fiber Soc 2001, 38, 644.
55. Martins, C. I.; Cakmak, M. SPE ANTEC 2004, 50, 2135.
56. Kim, K. H.; Isayev, A. I.; Kwon, K. J Appl Polym Sci, to appear.
57. Isayev, A. I.; Catignani, B. F. Polym Eng Sci 1997, 37, 1526.
58. Song, C. H.; Isayev, A. I. J Polym Eng 2000, 20, 427.
59. Evens, G. A. Practical Numerical Analysis; Wiley: New York, 1995.